Single Fiber Optical Coherence Tomography Microsurgical Instruments for Computer and Robot-Assisted Retinal Surgery

Marcin Balicki[1,*], Jae-Ho Han[1], Iulian Iordachita[1],
Peter Gehlbach[2], James Handa[2], Russell Taylor[1], and Jin Kang[1]

[1] ERC for Computer Integrated Surgery, Johns Hopkins University
[2] Wilmer Eye Institute, Johns Hopkins Medical, Baltimore, MD, USA
{marcin,iordachita,rht}@jhu.edu

Abstract. We present initial prototype and preliminary experimental demonstration of a new class of microsurgical instruments that incorporate common path optical coherence tomography (CP-OCT) capabilities. These instruments may be used freehand or with robotic assistance. We describe a prototype 25 gauge microsurgical pick incorporating a single 125 μm diameter optical fiber interfaced to a Fourier Domain CP-OCT system developed in our laboratory. For initial experimentation, we have interfaced this instrument with an extremely precise, cooperatively controlled robot. We describe the tool, system design, and demonstration of three control methods on simple phantom models: 1) enforcement of safety constraints preventing unintentional collisions of the instrument with the retinal surface; 2) the ability to scan the probe across a surface while maintaining a constant distance offset; and 3) the ability to place the pick over a subsurface target identified in a scan and then penetrate the surface to hit the target.

1 Introduction

Vitreoretinal surgery addresses prevalent sight-threatening conditions such as retinal detachment, macular pucker, macular holes, and conditions in which epiretinal scar tissue is removed. The technical demands placed on the surgeon by these procedures are extreme. In current practice, retinal surgery is performed under an operating microscope with free-hand instrumentation. Human limitations include an inability to clearly visualize surgical targets, physiological hand tremor, and lack of tactile feedback in tool-to-tissue interactions. In addition, tool limitations, such as lack of proximity sensing or smart functions, are important factors that contribute to surgical risk and reduce the likelihood of achieving surgical goals. Current instruments do not provide physiological or even basic interpretive information, e.g. the distance of the instrument from the retinal surface, the depth of instrument penetration into the retina or an indication of the force exerted by the instrument on the retinal tissues. Surgical outcomes (both success and failure) are limited, in part, by technical hurdles that cannot be overcome by current instrumentation. For example, in the most technically

[*] Supported in part by the NSF EEC9731748, NIH 1R01 EB007969-01 and ARCS Foundation.

G.-Z. Yang et al. (Eds.): MICCAI 2009, Part I, LNCS 5761, pp. 108–115, 2009.

demanding cases, there may not be a set of tools that allows the "typical" retina surgeon to remove sufficient epiretinal scar tissue to ensure surgical success.

In this paper, we will use the peeling of epiretinal membranes (ERMs) from the surface of the retina as a motivating example. ERM peeling is a common and extremely demanding surgical procedure. ERMs are composed of scar tissue that forms on the surface of the retina, contracts and compromises retinal function. ERMs are present in 2-6.4% of people [1]. Visual dysfunction resulting from ERM includes: blurred vision, image distortion, and altered image size. Surgical removal of an ERM involves identifying or creating an "edge" that is then grasped and peeled. Some ERMs provide clear visual evidence of edges that may be grasped. Others require creation of an edge by the surgeon. This may be performed by incising the membrane surface, by bluntly creating an edge, or by gently grasping the membrane with a forceps and creating a tear in the ERM. Each of these maneuvers requires excellent visualization, high levels of manual dexterity and micro-instrumentation. Furthermore, this procedure is performed with a comparatively large metal instrument without tactile sensation. During this time, a patient's involuntary and voluntary movement must be manually compensated for by the surgeon while the instrument is in direct contact with fragile intraocular tissue. Incorrect micron-magnitude movements can cause retinal tears, retinal detachment, visual field defects, retinal hemorrhage, local retinal edema, nerve fiber layer injury, and macular holes, all of which can contribute to blindness.

Optical Coherence Tomography (OCT) - provides very high resolution (micron scale) images of anatomical structures within the tissue. Within Ophthalmology, OCT systems typically perform imaging through microscope optics to provide 2D cross-sectional images ("B-mode") of the retina. These systems are predominantly used for diagnosis, treatment planning and in a few cases, for optical biopsy and image guided laser surgery [3-6].

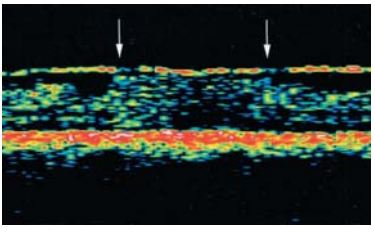

Fig. 1. Preoperative OCT scan of multiple points of retinal attachment (arrows) by epiretinal membrane [2]

Fig. 1 shows a typical OCT scan of an epiretinal membrane demonstrating multiple points of retinal attachment (arrows). ERMs are recognized by OCT as thin, highly reflective bands anterior to the retina. A potential dissection plane between the ERM and the retina is clearly visible in the scan, but is invisible to the surgeon through an operating microscope, even with very high magnification. In other work [7] our laboratory has explored registration of preoperative OCT images to intraoperative microscope images to aid in identifying ERM edges for initiating ERM removal. However, ERMs can grow and further distort retinal architecture. It is therefore, unclear whether preoperative images would provide a useful guide if the interval between the preoperative image acquisition and surgery allows for advancement of the ERM. Direct imaging of the ERM relative to the surgeon's instruments would be very useful either as a replacement for or supplement to the preoperative OCT images. In addition, direct imaging of the local anatomy relative to the instruments can be used to provide feedback on tool-to-tissue distances and real-time updates during tissue dissection.

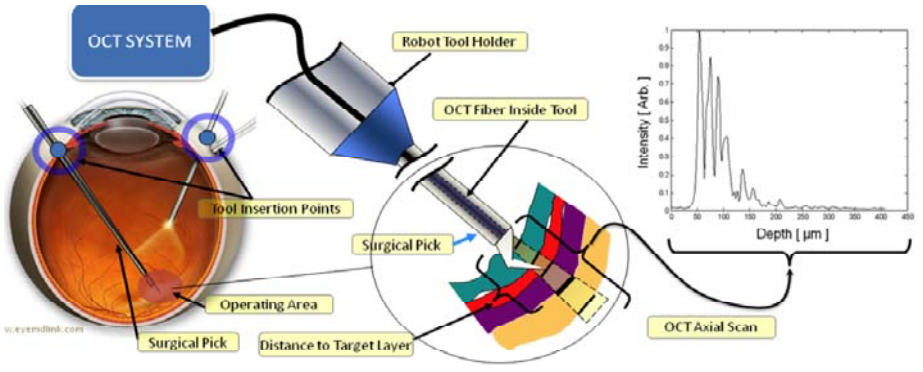

Fig. 2. Left: Proposed use of the instrument inside the human eye. Right: Axial OCT scan.

These considerations have led us to explore development of sub-millimeter diameter microsurgical instruments incorporating OCT sensing capability for directly sensing tissue planes beyond the instrument tip. Our approach (illustrated in Fig. 2) relies on the use of common path OCT (CP-OCT) sensing through an optical fiber built into the instrument shaft. Compared to alternative approaches, CP-OCT is simple, robust, and affordable [8], and also permits an extremely compact tool design. This "A-mode" sensing capability can either be used with conventional free-hand instruments or (as here) can be combined with a robotic microsurgery platform such as the JHU EyeRobot [9] or the CMU Micron [10]. When integrated with a robot, this instrument may be scanned to produce images of the local anatomy or integrated in various ways to the control the robot. This integration will allow design of a system that will have safety barriers that prevent collision with the retina, be able to maintain a constant distance from the retina during scanning, and be able to promote accurate targeting of anatomic features within the retina.

In this paper, we demonstrate integration of a single fiber OCT sensor into a 0.5 mm diameter microsurgical instrument designed for vitreoretinal surgical interventions. The instrument position is inherently registered to OCT by the fact that the surgical tip is visible in the OCT image. We have integrated this system into a robotic platform in order to investigate various control methods for its use in robotically assisted microsurgery.

2 Materials

OCT Integrated Pick Instrument. Vitreoretinal picks are commercially available in a variety of sizes with the most commonly used ranging from 25-20 gauge (0.5 mm to 0.9 mm diameter). Sharp picks are used to incise taut surface membranes and engage and elevate membrane edges for ERM peeling. The simplicity of this basic tool permits the surgeon to quickly craft a sharp edged pick from an appropriately sized surgical needle by bending the beveled tip with a needle holder. The surgeon co-authors routinely use this method to create such picks.

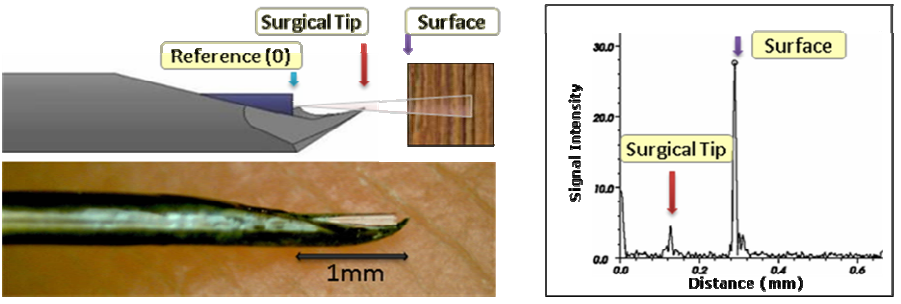

Fig. 3. Top Left: CAD side view of microsurgical pick with integrated fiber optic OCT probe. Bottom Left: Actual prototype. Right: A-Scan image of a sample.

For our experiments, we have adapted this method to permit incorporation of a single fiber OCT probe to enable simultaneous A-mode imaging and tissue manipulation. Our prototype picks were constructed from 25 gauge, 38mm surgical needles with 0.24mm ID and 0.5mm OD. We bent the beveled point approximately 200-300µm from the tip so that the tip intersected with the central axis of the needle lumen. A cleaved optical fiber stripped to glass cladding was inserted through the lumen, bonded in place approximately 135µm from the tip, and interfaced to the CP-OCT system. The tip is visible in the OCT A-mode image, thus providing a reference point for the relative distance of the tool to tissue being scanned (Fig. 3).

Optical Coherence Tomography System. The optical fiber from the tool is integrated with a common path Fourier domain OCT system developed in our laboratory and is fully described in [8]. It is the simplest, most compact imaging technique of its kind. This system is robust, inexpensive, and can utilize simple interchangeable probes. Our system uses an SLED light source centered near 0.8-µm wavelength with a fiber optic directional 2x2 coupler, and a USB spectrometer (HR4000, Ocean Optics Inc.). The optical fiber probes presented here are a single mode fiber (NA 0.14) with ~9µm core size, 125µm cladding diameter and ~245µm diameter outer polymer buffer. The imaging depth is 1-1.5 mm in tissue and somewhat less in our wax sample materials. In air, the OCT beam diverges at an angle of 16 degrees and effective axial resolution is ~8.8µm. In water or tissue the divergence is ~12 degrees with ~6.6 µm resolution. A sample axial image (A-Mode) with zero reference point located at the tip of the fiber is shown in Fig. 2. By moving the probe laterally, a sample cross section image is generated (B-Mode).

The CP-OCT system provided the robot with the distance from the probe to the surface of the sample. Each axial scan was processed by first thresholding to remove baseline noise, and then smoothing with a Savitzky-Golay filter to preserve peak locations, amplitudes and widths. To locate the peaks, a simple zero-crossing of signal derivative was used. The acquisition time and signal processing yields a sampling rate of ~200Hz with approximate latency of one frame.

Sample materials. We have developed two artificial phantoms for consistent evaluation in these preliminary experiments. For the safety barrier and surface tracking tasks, we use a composite of three 60µm thick layers of scotch tape on a dense

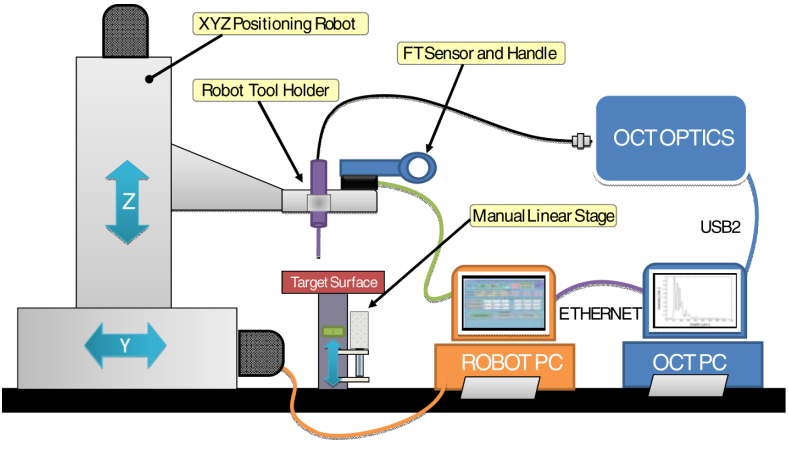

Fig. 4. Experimental system overview

wooden plank. This provides a strong multi-peak axial scan signal that is analogous to that generated by the multilayered structures of the retina. For the targeting tasks, we needed a phantom with 100-300µm diameter cavities located near the surface and the ability to display any physical interaction with the sample. Sheet lining wax (McMaster 8691K31) with a low softening point (135°C) was placed on an aluminum sheet and heated to boiling. Rapid cooling produces many thin-walled bubbles and any physical contact between the pick and sample surface leaves permanent marks visible in OCT.

Experimental Setup. Our experimental setup is illustrated in Fig. 4. The microsurgical instrument is mounted on an extremely precise Cartesian positioning robot consisting of three orthogonally mounted linear stages. The position resolution is 1µm and measured repeatability is about ± 1 µm for range of motion required for this experiment (<2mm). This robot was chosen for experimental convenience, and would be replaced in actual practice by a system similar to [9-10]. The robot is interfaced to a PC workstation through a commercial motion controller (Galil DMC 1886). A commercial 6 DOF force-torque sensor (ATI Nano43) is mounted on the robot and also interfaced to the PC as a user interface. Open-source robot control software developed in our laboratory [11] is used to implement cooperative "hands on" control for the robot's motion. The OCT system is implemented on a separate PC and communicates to the robot PC via Ethernet. The test samples are mounted on a separate manually actuated micrometer stage placed beneath the probe. An inspection video microscope (Omano E-ZVU/V15) is positioned to simultaneously image the side view of the sample and probe at 90X magnification (not shown).

3 Methods

We have demonstrated our system in the context of three sample tasks: enforcement of safety barriers, "tracking" to maintain a constant distance from a surface, and accurate placement of the probe on targets identified in a scanned OCT image. Relatively

low velocities were chosen based on surgical preference when operating close to the retina and the limited movement in the eye during surgery due to constraints by insertion of tools through the sclera and effects of anesthetics.

In the **safety barrier** task, the system enforced a safety constraint to prevent the probe from approaching the target surface closer than a specified threshold distance. The robot moved freely within the 1D workspace to comply with forces exerted by the user on the control handle, with the exception of the forbidden boundary sensed via the OCT. This "virtual wall" was reached when the tip of the probe was located ~150µm from the sample surface. A bare optical fiber was used as a probe. Five trials were performed with different robot velocity limits: 100, 200, 300, 400, 500 µm/sec.

In the **surface tracking** task, the sample surface was moved up and down with the manual micrometer stage while the robot was controlled to maintain a constant OCT-reported distance of 150 µm from the sample surface. One intention for the surface tracking was to correct for retinal motion due to respiratory function, hence we chose the sinusoidal frequency to be around 0.2 Hz and magnitude that encompasses expected ranges of retinal motion.

In the **targeting** task, the robot was instructed to scan the pick in 2µm increments laterally across the sample surface. The A-mode images from the OCT system were then combined to make a B-mode image. The evolving B-mode image was displayed continuously to the user, who could use a mouse at any time to click on a target within the image. The robot would then interrupt its scan, move back to a position over the identified target, and then slowly insert the pick tip to the depth of the designated target, based on depth feedback provided by the OCT system. The probe was then withdrawn and a second B-mode scan was taken to observe the created defect in the sample surface.

4 Results

The results for the safety barrier task are shown in Fig. 5(left). The observed overshoot into the "unsafe" zone was negligible for robot speeds up to ~300 µm/sec and still quite modest up to ~500 µm/sec, using only a very naïve control method. Further improvements are expected with our next generation OCT system (which has higher sample rate) and with refinements in the robot design and control.

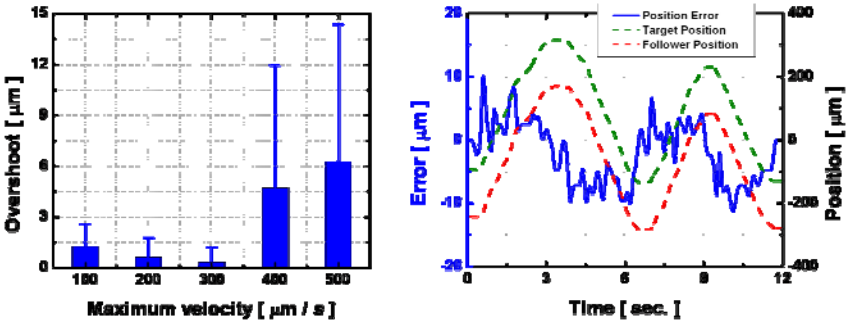

Fig. 5. Results: Left: Safety Barrier - Overshoot error vs. maximum allowable velocity. Right: Surface tracking with 150µm standoff.

The results of dynamic response when tracking sinusoidal surface motion are shown in Fig. 5(right). We were able to keep the tool tip within about 10 µm of the desired 150 µm standoff from the target surface while the surface moved at about 200 µm/sec.

The results of the targeting task are illustrated in Fig. 6. The top B-Scan shows a subsurface bubble with 30-50µm membrane and the user specified incision location. The bottom shows the post-intervention B-Scan with an overlay depicting approximate orientation and location of the instrument tip at the target. The defect clearly resembles the geometry of the tip, as well as good alignment with planned incision position.

5 Discussion and Future Work

"Smart" instruments combining real time sensing with tissue manipulation have significant potential to improve surgical practice, especially when combined with real time visualization, robotic devices, and computer-based decision support. In this paper, we have introduced a new class of microsurgical instruments for retinal surgery, incorporating fiber-optic common path Fourier domain OCT sensing. Although the development of such instruments and techniques for using them is still in early stages, our initial experiments are very encouraging.

We have found that very small instruments (~0.5mm diameter) incorporating fiber-optic OCT can be constructed and used to identify tissue boundaries beyond the tip of the instruments. Further, the instrument can be scanned laterally to construct 2D and 3D images from the single A-mode images produced by the basic sensor. We have demonstrated that the sensor can provide real time feedback on the distance from the tool tip to a surface and can be used to enforce safety barriers or support surface following with a robot. Finally, we have shown that these capabilities can be combined to enable user identification of a subsurface target in a scanned image followed by automated placement of the instrument tip on the target. All of these capabilities will be very useful in future clinical vitreoretinal systems.

Further development will require us to address a number of technical and practical questions. The current experiments were performed with the probe perpendicular to the sample surface. Although OCT can identify layers while looking obliquely into tissue at the angles that will be encountered in retinal surgery, it is still necessary to account for approach angle to get correct range data. We are developing several approaches to address this, such as robot pose

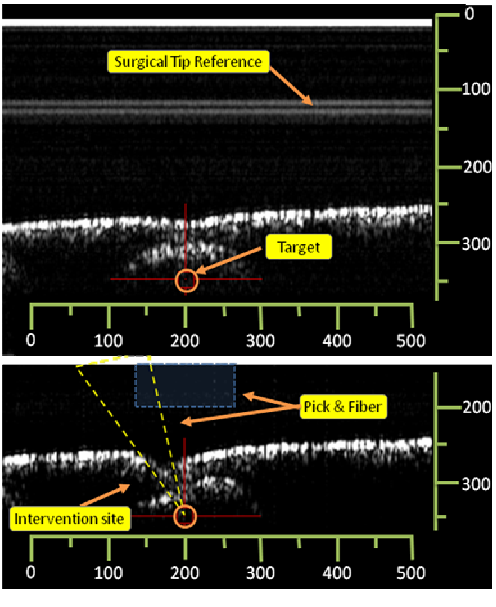

Fig. 6. B-Mode scan before and after intervention

feedback and tracking of tools in the stereo video microscope. Practical issues include: fabrication processes, optical path occlusion by stray particles in the microenvironment, improvement in the speed of OCT data acquisition, and interfacing to our surgical robots. None of these seem insuperable, though experimentation and design iteration will be needed. For example, we need to determine if particle occlusion is a problem within the aqueous environment of the eye, or if the particles simply wash off.

In the immediate future, we will pursue several paths. First, we have just completed a new CP-FDOCT system with considerably higher performance. After repeating the experiments described above, we will begin evaluating the combined system with multiple tissue samples in our lab and will also interface the system to the microsurgical robots in our lab. In the intermediate term, we will also develop methods for tracking instruments in the surgical microscope, for making the necessary depth corrections, for producing B-mode images from the tracked tool positions, and for generating registered overlaid displays on the microscope.

References

1. Sjaarda, R.N., Michels, R.G.: Macular pucker. In: Ryan, S.J. (ed.) Retina, 2nd edn., Mosby, St. Louis, vol. 3, pp. 2301–2312 (1994)
2. Keisuke, M., Gehlbach, P.L., SanoA., D.T., Yoneya, S.: Comparison of Epiretinal Membranes of Differing Pathogenesis Using Optical Coherence Tomography. Retina 24, 57–62 (2004)
3. Fujimoto, J.G., Pitris, C., Boppart, S.A., Brezinski, M.E.: Optical coherence tomography: an emerging technology for biomedical imaging and optical biopsy. Neoplasia 2(1-2), 9–25 (2000)
4. Herrmann, J.M., Boppart, S.A., Bouma, B.E., Tearney, G.J., Pitris, C., Brezinski, M.E., Fujimoto, J.G.: Real time imaging of laser intervention with optical coherence tomography. In: Biomedical Optical Spectroscopy and Diagnostics / Therapeutic Laser Applications. OSA Trends in Optics and Photonics Series, paper TSuD2, vol. 22 (1998)
5. Boppart, S.A., Nguyen, F.T., Zysk, A.M., Chaney, E.J., Kotynek, J.G., Oliphant, U.J., Bellafiore, F.J., Rowland, K.M., Johnson, P.A.: Coherent optical imaging and guided interventions in breast cancer: translating technology into clinical applications. In: Proc. SPIE, vol. 6991, 699102 (2008)
6. Han, S., Sarunic, M.V., Wu, J., Humayun, M., Yang, C.: Handheld forward-imaging needle endoscope for ophthalmic optical coherence tomography inspection. J. Biomed. Opt. 13, 20505 (2008)
7. Fleming, I.N., Voros, S., Vagvolgyi, B., Pezzementi, Z., Handa, J., Taylor, R., Hager, G.D.: Intraoperative Visualization of Anatomical Targets in Retinal Surgery. In: Fleming, I.N., Voros, S., Vagvolgyi, B., Pezzementi, Z., Handa, J., Taylor, R., Hager, G.D. (eds.) IEEE Workshop on Applications of Computer Vision, 2008. WAC 2008, January 7-9, 2008, pp. 1–6 (2008)
8. Liu, X., Li, X., Kim, D.-H., Ilev, I., Kang, J.U.: Fiber Optic Fourier-domain Common-path OCT. C. Optics Letters 06(12), 899–903 (2008)
9. Mitchell, B., Koo, J., Iordachita, I., Kazanzides, P., Kapoor, A., Handa, J., Hager, G., Taylor, R.: Development and Application of a New Steady-Hand Manipulator for Retinal Surgery. IEEE ICRA, 623–629 (2007)
10. Riviere, W.A., Khosla, P.: Toward active tremor canceling in handheld microsurgical instruments. IEEE Trans. Rob. Autom. 19, 793–800 (2003)
11. Kapoor, A., Deguet, A., Kazanzides, P.: Software components and frameworks for medical robot control. In: IEEE ICRA, pp. 3813–3818 (2006)